AIAA-2002-3888

Application of the Space-Time Conservation Element and Solution Element Method to the Ideal Magnetohydrodynamic Equations

Moujin Zhang[1], S.-C. Henry Lin[2], S.-T. John Yu[3]
Mechanical Engineering Department
Wayne State University, Detroit, MI 48202

Sin-Chung Chang[4] and Isaiah Blankson[5]
NASA Glenn Research Center
Cleveland, OH 44135

Abstract

In this paper, we introduce a new numerical approach to solve the MHD equations by the space-time Conservation Element and Solution Element (CESE) method. By treating space and time as one entity, the ideal MHD equations are formulated in a space-time integral form, and are solved by the CESE method. As a contrast to the modern upwind methods, no reconstruction procedure or Riemann solver is needed in the present approach. The computational logic and operational count of the present approach are much simpler and more efficient. Preliminary results of propagating MHD shock and expansion waves in one and two spatial dimensions showed remarkable numerical resolution.

1. Introduction

Recently, computational magneto-hydrodynamics (MHD) has drawn significant attention as a means to access the viability of several advanced propulsion concepts, including drag reduction by a weakly ionized plasma engulfing propulsion vehicles, and the AJAX concept, which could offer significantly higher exhaust kinetic energy than that of chemical propulsion systems for hypersonic propulsion. In this paper, we are concerned with the ideal MHD equations, which are derived based on the Euler equations for flow motions in conjunction with the Maxwell equations for the electromagnetic (EM) fields. Due to evolving body forces by the EM fields, wave structures in plasma flows are much more complex than that in gas dynamics.

To date, the standard approach to solve MHD problems has been based on the use of modern upwind schemes [1-7], in which the main efforts is the development of a viable Riemann solver based on the knowledge about the eigensystem of the flow equations. Moreover, for computational efficiency, further approximation of the Riemann solvers employed is often developed. However, unlike the gas dynamics equations, to which analytical solution in one spatial dimension is well-known, available analytical solutions to the MHD waves have been scant. Therefore, the development of approximate Riemann solvers for

[1] Research Associate, Email: mzhang@me1.eng.wayne.edu
[2] Ph.D. Candidate, Email:memsworld@yahoo.com
[3] Associate Professor, Email: styu@me1.eng.wayne.edu
[4] Senior Aerospace Scientist, Email: sin-chung.chang@lerc.nasa.gov
[5] Senior Technologist, Email: isaiah.blankson@lerc.nasa.gov

MHD equations involves many theoretical uncertainties. When extending to plasma flows in multiple spatial dimensions, the common practices in upwind methods are based on directional splitting, i.e., waves propagating in a multi-dimensional space are approximated by superposition of one-dimensional Riemann solutions from each of the orthogonal directions. While the practice is standard in calculating gas dynamics equations, direct extension of this treatment for complex MHD equations need further study.

In a series of publications [8-12], Chang and coworkers have successfully developed a new numerical framework for linear and nonlinear convection-diffusion equations in one, two, and three spatial dimensions. Numerous results, obtained by using the CESE method, have been reported, including flows with steady and moving shock, rarefaction waves, and acoustic waves, flows dominated by vortices, detonating flows, shock/acoustic waves/vortices interactions, dam-break flows, hydraulic jump, cavitating flows, and the turbulent flows with embedded sprays.

Due to the complexity of the MHD problems, highly accurate but simple method is desired. In this paper, we use the Space-time CESE method [8-12] to solve the ideal MHD equations. Contrast to modern upwind methods, the CESE method does not use a Riemann solver or a reconstruction step as building blocks. The logics and operational count are much simpler. This effort is only a steppingstone for further development of the CESE method as a general numerical framework for complex MHD models.

The rest of the paper is organized as follows. Section 2 illustrates the model equations. Section 3 briefly reviews the CESE method and its application to solve the MHD equations. In Section 4, numerical results are presented. Standard tests of one- and two-dimensional MHD flows are presented. In addition, we also show that the non-reflective condition treatment by the CESE method could be straightforwardly implemented for the MHD equations, and the treatments would allow shock waves to propagate out of the computational domain. We then offer concluding remarks and provide cited references.

2. Model Equations

By neglecting displacement current, electrostatic forces, effects of viscosity, resistivity and heat conduction, the one-dimensional system of MHD equations has the following form:

$$\frac{\partial \mathbf{u}}{\partial t} + \frac{\partial \mathbf{f}}{\partial x} = 0 \tag{2.1}$$

where

$$\mathbf{u} = \left[\rho, \rho u, \rho v, \rho w, e, B_y, B_z\right]^T \tag{2.2}$$

and

$$\mathbf{f}(\mathbf{u}) = \begin{bmatrix} \rho u \\ \rho u^2 + p_0 - \frac{B_x^2}{4\pi} \\ \rho uv - \frac{B_x B_y}{4\pi} \\ \rho uw - \frac{B_x B_z}{4\pi} \\ (e + p_0)u - \frac{(uB_x + vB_y + wB_z)u}{4\pi} \\ uB_y - vB_x \\ uB_z - wB_x \end{bmatrix} \tag{2.3}$$

where ρ is the density, p is the static pressure, *(u, v, w)* are the fluid velocity components in the *x, y,* and *z* directions, respectively, B_x, B_y and B_z are components of the magnetic field in the *x, y* and *z* directions, respectively, and γ is the ratio of specific heats. The total energy per unit volume is defined as

$$e = p/(\gamma - 1) + \rho(u^2 + v^2 + w^2)/2 + (B_x^2 + B_y^2 + B_z^2)/8\pi$$

The total pressure is

$$p_0 = p + (B_x^2 + B_y^2 + B_z^2)/8\pi .$$

In addition to the above equations, we must have $\nabla \bullet \vec{\mathbf{B}} = 0$, which is satisfied in the initial condition.

The Jacobian matrix *F* of ideal one-spatial dimensional MHD equations and is listed in the Appendix. The Jacobian matrix has seven real

eigenvalues: $u-c_f, u-c_a, u-c_s, u, u+c_s, u+c_a$ and $u+c_f$, where c_a, c_f and c_s are Alfven, fast and slow characteristic speeds respectively, and can be expressed as

$$c_a = |B_x| / \sqrt{4\pi\rho} \tag{2.4a}$$

$$c_{f,s} = \frac{1}{2}\left[\sqrt{c^2 + \frac{\mathbf{B}\bullet\mathbf{B}}{4\pi\rho} + \frac{|B_x|c}{\sqrt{\pi\rho}}} \pm \sqrt{c^2 + \frac{\mathbf{B}\bullet\mathbf{B}}{4\pi\rho} - \frac{|B_x|c}{\sqrt{\pi\rho}}}\right] \tag{2.4b}$$

$$c^2 = \gamma p/\rho \tag{2.4c}$$

Note, unlike the Jacobian matrix for pure gas dynamics, the present MHD Jacobian matrix is not homogenous, i.e., $\mathbf{f} \neq F\mathbf{u}$. This prevents the use of a simplified version of the $a-\varepsilon$ scheme in the CESE method family for the MHD problems. The details will be provided in the following section.

3. The CESE Method

In this Section, we first review the basic ideas and implementation steps of the CESE method. We then apply the CESE method to the MHD equations.

3.1 Review of the CESE method for one-dimensional flow problem

The general conservation form of a nonlinear system can be express as follows,

$$\frac{\partial \mathbf{u}}{\partial t} + \frac{\partial \mathbf{f}}{\partial x} = 0 \tag{3.1}$$

The basic ideas and characters of the CESE method for solving such a system was summarized as the following steps:

1) Constructing Solution Element (SE) and Conservation Element (CE) based on unity of space and time.

A staggered grid point arrangement is employed in the space-time coordinate as shown in Figure 1a. The index j refers to the spatial direction and the index n to the time direction. Based on the grid point arrangement, the solution element $SE(j,n)$ defined for point (j,n) is enclosed by dashed curves as shown in Figure 1b. It includes a vertical line segment, a horizontal line segment and their immediate neighborhood. A SE is very close to, but not contact with the others in spatial and time direction. The surface of two SE forms one CE as shown in Figure 1c. That is, surfaces of $SE(j,n)$ and $SE\left(j-\frac{1}{2}, n-\frac{1}{2}\right)$ form the $CE\_(j,n)$, while surface of $SE(j,n)$ and $SE\left(j+\frac{1}{2}, n-\frac{1}{2}\right)$ form the $CE_+(j,n)$. Based on this treatment, the time and space are treated as an entity. This is the key difference between the CESE method and traditional numerical methods.

2) Specifying primitive parameters' profiles with Taylor's expansion.

Inside the $SE(j,n)$, the parameters' distribution is assumed as smooth and follows the first-order Taylor series expansion as,

$$\mathbf{u}^* = \mathbf{u}_j^n + (\mathbf{u}_x)_j^n (x-x_j) + (\mathbf{u}_t)_j^n \left(t-t^n\right) \tag{3.2}$$

As an analog, the flux's distribution inside a SE also follows the similar correlation as,

$$\mathbf{f}^* = \mathbf{f}_j^n + (\mathbf{f}_x)_j^n (x-x_j) + (\mathbf{f}_t)_j^n \left(t-t^n\right) \tag{3.3}$$

Where $(\mathbf{u})_j^n, (\mathbf{u}_x)_j^n, (\mathbf{u}_t)_j^n, (\mathbf{f}_x)_j^n$ and $(\mathbf{f}_t)_j^n$ are defined as constants inside $SE(j,n)$ and refer to the values at grid point (j,n). The last term $(\mathbf{f}^v)_j^n$, defined by $(\mathbf{u})_j^n$ and $(\mathbf{u}_x)_j^n$, is treated as a constant inside $SE(j,n)$.

Substituting Eqs. (3.2) and (3.3) into Eq. (3.1), we yield,

$$(\mathbf{u}_t)_j^n = -(\mathbf{f}_x)_j^n \tag{3.4}$$

Since $(\mathbf{f})_j^n$ is a function of $(\mathbf{u})_j^n$, $(\mathbf{f}_x)_j^n$ can be further expressed by product of Jacobian matrix F defined by $(\mathbf{u})_j^n$ and $(\mathbf{u}_x)_j^n$ as

$$\left(\mathbf{f}_x\right)_j^n = \left(F\right)_j^n \left(\mathbf{u}_x\right)_j^n \tag{3.5a}$$

Eq.(3.4) can be further expressed as

$$\left(\mathbf{u}_t\right)_j^n = -\left(F\right)_j^n \left(\mathbf{u}_x\right)_j^n \tag{3.5b}$$

With Eq. (3.3), $\left(\mathbf{f}_t\right)_j^n$ is also expressed by $\left(\mathbf{u}\right)_j^n$ and $\left(\mathbf{u}_x\right)_j^n$ in a similar way as

$$\left(\mathbf{f}_t\right)_j^n = \left(F\right)_j^n \left(\mathbf{u}_t\right)_j^n = -\left(F\right)_j^n \left(F\right)_j^n \left(\mathbf{u}_x\right)_j^n \tag{3.5c}$$

That is, Eqs. (3.2) and (3.3) can be further expressed by $\left(\mathbf{u}\right)_j^n$ and $\left(\mathbf{u}_x\right)_j^n$. In the CESE method the first-order-spatial-derivatives $\left(\mathbf{u}_x\right)_j^n$ are introduced as solving variables. This is the second difference between the CESE method and other numerical methods. Note, the physical parameters are defined to have smooth profiles inside a SE, while between SEs or in CEs, they may be disconnected. That is the key reason why the CESE method can capture sharp discontinuity within few grid points.

3) Obtaining an explicit marching scheme based on local flux conservation.

Let x and t be coordinates of a two-dimensional Eucilidean space E_2 and by using Gauss' divergence theorem, the corresponding integral conservation form of Eq. (3.1) is as follows,

$$\oint_{S(V)} \mathbf{h} \bullet d\mathbf{s} = 0 \tag{3.6}$$

where $\mathbf{h} = \left(\mathbf{f}, \mathbf{u}\right)$ is the current density vector in E_2 space, and S is the surface of a space-time volume V.

Applying Eq.(3.6) to $CE_+\left(j,n\right)$ and $CE_-\left(j,n\right)$ respectively, while substituting Eqs. (3.2) and (3.3), two sets of equations can be obtained. Obviously, the equations consist of $\left(\mathbf{u}\right)_j^n$, $\left(\mathbf{u}_x\right)_j^n$, $\left(\mathbf{u}\right)_{j\pm\frac{1}{2}}^{n-\frac{1}{2}}$ and $\left(\mathbf{u}_x\right)_{j\pm\frac{1}{2}}^{n-\frac{1}{2}}$. For unknowns $\left(\mathbf{u}\right)_j^n$ and $\left(\mathbf{u}_x\right)_j^n$, the two sets of equations are linear algebraic ones, and it is straightforward to obtain their expressions respectively to form an explicit marching scheme. This scheme is named as the *a* scheme for Eq.(3.1).

The detailed expressions for convective-diffusive equation were rigorously derived in [9]. Here the expressions for Eq. (3.1) were given through Eqs.(3.7) to (3.10). The derivation is just the same as that for convective-diffusive equation.

$$\mathbf{u}_j^n = \frac{1}{2}\left[\mathbf{u}_{j+1/2}^{n-1/2} + \mathbf{u}_{j-1/2}^{n-1/2} + \mathbf{s}_{j-1/2}^{n-1/2} - \mathbf{s}_{j+1/2}^{n-1/2}\right] \tag{3.7}$$

$$\frac{\Delta x}{4}\left(\mathbf{u}_x\right)_j^n + \frac{\left(\Delta t\right)^2}{4\Delta x}\left(\mathbf{f}_t\right)_j^n = \mathbf{b}_j^n \tag{3.8}$$

where

$$\mathbf{s}_j^n = \frac{\Delta x}{4}\left(\mathbf{u}_x\right)_j^n + \frac{\Delta t}{\Delta x}\left(\mathbf{f}\right)_j^n + \frac{\left(\Delta t\right)^2}{4\Delta x}\left(\mathbf{f}_t\right)_j^n \tag{3.9}$$

$$\mathbf{b}_j^n = \frac{\Delta t}{\Delta x}\left(\mathbf{f}\right)_j^n + \frac{1}{2}\left[\mathbf{u}_{j+1/2}^{n-1/2} + \mathbf{u}_{j-1/2}^{n-1/2} - \mathbf{s}_{j-1/2}^{n-1/2} - \mathbf{s}_{j+1/2}^{n-1/2}\right] \tag{3.10}$$

4) Introducing adjustable numerical dissipation to obtain a stable solution.

The a scheme is neutrally stable and reversible in time, and generally becomes unstable when discontinuity appears. For most cases of flow problem, the $a-\mu$ scheme becomes unstable, even the physical viscosity has some damping effect on discontinuity. To overcome this problem, an adjustable parameter ε, which is independent of numerical variables, is added to the present marching scheme to form a $a-\varepsilon$ scheme. The introducing of ε to scalar convective-diffusive equations and its effect on numerical result and stability are discussed in detail in [11].

As an analog, the same form for introducing ε is employed for vector $\left(\mathbf{u}_x\right)_j^n$ as,

$$\left(\mathbf{u}_x\right)_j^n = \left(\mathbf{u}_x^a\right)_j^n + 2\varepsilon\left[\left(\mathbf{u}_x^c\right)_j^n - \left(\mathbf{u}_x^a\right)_j^n\right] \tag{3.11}$$

where $\left(\mathbf{u}_x^a\right)_j^n$ refers to $\left(\mathbf{u}_x\right)_j^n$ obtained from Eq.(3.8). $\left(\mathbf{u}_x^c\right)_j^n$ is calculated based on a central differencing as,

$$\left(\mathbf{u}_x^c\right)_j^n = \frac{1}{2}\left[\left(\mathbf{u}_{x+}^c\right)_j^n + \left(\mathbf{u}_{x-}^c\right)_j^n\right] \tag{3.12a}$$

$$\left(\mathbf{u}_{x\pm}^{c}\right)_j^n = \pm\frac{1}{2}\left(\mathbf{u}'^{n}_{j\pm1/2} - \mathbf{u}_j^n\right) \tag{3.12b}$$

$$\mathbf{u}'^{n}_{j\pm1/2} = \mathbf{u}^{n-1/2}_{j\pm1/2} + \frac{\Delta t}{2}\left(\mathbf{u}_t\right)^{n-1/2}_{j\pm1/2} \tag{3.12c}$$

Note: the parameter ε only appears in the marching scheme for $\left(\mathbf{u}_x\right)_j^n$, while the marching scheme for $\left(\mathbf{u}\right)_j^n$ is independent of ε. In fact, obtaining $\left(\mathbf{u}_x\right)_j^n$ is the key point to implement CESE method.

The second part in the right side of Eq. (3.11) is to introduce an artificial dissipation to damp out numerical instability that arises from the smooth region of a solution. But it is less effective in suppressing numerical wiggles that often occur near a discontinuity. For more generality, a further modification is made to obtain a $a-\varepsilon-\alpha-\beta$ scheme as,

$$\begin{aligned}\left(\mathbf{u}_x\right)_j^n = \left(\mathbf{u}_x^a\right)_j^n &+ 2\varepsilon\left[\left(\mathbf{u}_x^c\right)_j^n - \left(\mathbf{u}_x^a\right)_j^n\right] \\ &+ \beta\left[\left(\mathbf{u}_x^w\right)_j^n - \left(\mathbf{u}_x^c\right)_j^n\right]\end{aligned} \tag{3.13}$$

where

$$\left(\mathbf{u}_x^w\right)_j^n = W_0\left[\left(\mathbf{u}_{x+}^c\right),\left(\mathbf{u}_{x-}^c\right);\alpha\right] \tag{3.14a}$$

$$W_0\left(x_-,x_+;\alpha\right) = \frac{\left|x_+\right|^\alpha x_- + \left|x_-\right|^\alpha x_+}{\left|x_+\right|^\alpha + \left|x_-\right|^\alpha} \tag{3.14b}$$

Three parameters, ε, α and β, are introduced to obtain the $a-\varepsilon-\alpha-\beta$ scheme. If their values are chosen properly, the present general scheme can handle both small disturbances and sharp discontinuities. For most cases solved by the CESE method, the parameters α and β were all set to unity, even they can be considered as functions of local dynamical variables and mesh parameters in [9]. Note that the third difference between the CESE method and most numerical methods is the introduced damping effect is controllable.

Besides the above schemes, Chang also presented a simplified $a-\varepsilon$ scheme for Euler equations in [9] (i.e. Eq. (4.28) in [9]). The detailed derivation is as follows,

Rewriting the $a-\varepsilon$ scheme for convective scalar equation (i.e. Eq.(3.10) in [9]) as,

$$\begin{aligned}\left(u_x\right)_j^n = \frac{1}{\Delta x}&\left[\left(u_x\right)_{j+1/2}^{n-1/2} - \left(u_x\right)_{j-1/2}^{n-1/2}\right] \\ &+ \left(2\varepsilon-1\right)\left(du_x\right)_j^n\end{aligned} \tag{3.15}$$

where

$$\begin{aligned}\left(du_x\right)_j^n = \frac{1}{2}&\left[\left(u_x\right)_{j+1/2}^{n-1/2} + \left(u_x\right)_{j-1/2}^{n-1/2}\right] \\ &- \frac{1}{\Delta x}\left(u_{j+1/2}^{n-1/2} - u_{j-1/2}^{n-1/2}\right)\end{aligned} \tag{3.16}$$

Note that if ε is set to zero, Eq.(3.15) is exactly the a scheme for convective scalar equation, that is derived from scalar form of Eq.(3.8).

As an analogy for vector equation as Eq.(2.1), the Eq(3.15) can be recast in the same vector form as

$$\begin{aligned}\left(\mathbf{u}_x\right)_j^n = \frac{1}{\Delta x}&\left[\left(\mathbf{u}_x\right)_{j+1/2}^{n-1/2} - \left(\mathbf{u}_x\right)_{j-1/2}^{n-1/2}\right] \\ &+ \left(2\varepsilon-1\right)\left(\mathbf{du}_x\right)_j^n\end{aligned} \tag{3.17}$$

where

$$\begin{aligned}\left(\mathbf{du}_x\right)_j^n = \frac{1}{2}&\left[\left(\mathbf{u}_x\right)_{j+1/2}^{n-1/2} + \left(\mathbf{u}_x\right)_{j-1/2}^{n-1/2}\right] \\ &- \frac{1}{\Delta x}\left(\mathbf{u}_{j+1/2}^{n-1/2} - \mathbf{u}_{j-1/2}^{n-1/2}\right)\end{aligned} \tag{3.18}$$

If Eq.(3.17) is valid, the Eq.(3.17) with setting ε to zero should be derived exactly from Eq.(3.8). Actually, for Euler equation and with an assumption, it is valid.

Since for Euler equations, we have,

$$\mathbf{f}_j^n = F_j^n\mathbf{u}_j^n \tag{3.19}$$

Substituting Eqs. (3.5c) and (3.15) into Eq.(3.8), we yield,

$$\begin{aligned}\left(\mathbf{u}_x\right)_j^n = \frac{2}{\Delta x}&\left[\left(I - V_j^n\right)^{-1}\left(I - V_{j+1/2}^{n-1/2}\right)\mathbf{u}_{j+1/2}^{n-1/2}\right. \\ &\left. - \left(I + V_j^n\right)^{-1}\left(I + V_{j-1/2}^{n-1/2}\right)\mathbf{u}_{j-1/2}^{n-1/2}\right] \\ &- \frac{1}{2}\left\{\left(I - V_j^n\right)^{-1}\left[I - \left(V_{j+1/2}^{n-1/2}\right)^2\right]\left(\mathbf{u}_x\right)_{j+1/2}^{n-1/2}\right. \\ &\left. + \left(I + V_j^n\right)^{-1}\left[I - \left(V_{j-1/2}^{n-1/2}\right)^2\right]\left(\mathbf{u}_x\right)_{j-1/2}^{n-1/2}\right\}\end{aligned} \tag{3.20}$$

where, I is the unit matrix and $V_j^n = \frac{\Delta t}{\Delta x} F_j^n$

With the following assumptions as

$$F_j^n = F_{j+1/2}^{n-1/2} = F_{j-1/2}^{n-1/2} \tag{3.21}$$

With the aid of Eq.(3.5b), equation (3.20) can be further simplified as

$$\begin{aligned}
(\mathbf{u}_x)_j^n &= \frac{2}{\Delta x}\left[\mathbf{u}_{j+1/2}^{n-1/2} - \mathbf{u}_{j-1/2}^{n-1/2}\right] \\
&\quad - \frac{1}{2}\left[\left(I + V_{j+1/2}^{n-1/2}\right)(\mathbf{u}_\mathbf{x})_{j+1/2}^{n-1/2}\right. \\
&\quad \left. + \left(I - V_{j-1/2}^{n-1/2}\right)(\mathbf{u}_\mathbf{x})_{j-1/2}^{n-1/2}\right] \\
&= \frac{1}{\Delta x}\left[\mathbf{u}_{j+1/2}^{n-1/2} - \mathbf{u}_{j-1/2}^{n-1/2}\right] \\
&\quad - \frac{1}{2}\left[(\mathbf{u}_\mathbf{x})_{j+1/2}^{n-1/2} + (\mathbf{u}_\mathbf{x})_{j-1/2}^{n-1/2}\right] \\
&\quad + \frac{1}{\Delta x}\left[\mathbf{u}_{j+1/2}^{n-1/2} - \mathbf{u}_{j-1/2}^{n-1/2}\right] \\
&\quad - \frac{1}{2}\left[V_{j+1/2}^{n-1/2}(\mathbf{u}_\mathbf{x})_{j+1/2}^{n-1/2} - V_{j-1/2}^{n-1/2}(\mathbf{u}_\mathbf{x})_{j-1/2}^{n-1/2}\right] \\
&= \frac{1}{\Delta x}\left\{\left[\mathbf{u}_{j+1/2}^{n-1/2} - \frac{\Delta t}{2} F_{j+1/2}^{n-1/2}(\mathbf{u}_\mathbf{x})_{j+1/2}^{n-1/2}\right]\right. \\
&\quad \left. - \left[\mathbf{u}_{j-1/2}^{n-1/2} - \frac{\Delta t}{2} F_{j-1/2}^{n-1/2}(\mathbf{u}_\mathbf{x})_{j-1/2}^{n-1/2}\right]\right\} \\
&\quad - (\mathbf{du}_x)_j^n \\
&= \frac{1}{\Delta x}\left[(\mathbf{u})_{j+1/2}^{n-1/2} - (\mathbf{u})_{j-1/2}^{n-1/2}\right] - (\mathbf{du}_x)_j^n
\end{aligned} \tag{3.22}$$

Eq.(3.22) is the Eq.(3.17) with ε setting to zero. For a homogenous Jacobian matrix and with assumption of Eq.(3.21), the Eq.(3.17) can be used for systems like Eq.(2.1). That is the origin of Eq. (4.28) in [9]. Comparing with Eq. (3.13), Eq. (3.17) is much more easier to implement for solving Euler equations. According to our experience, the Eq. (3.17) is good enough for solving Euler equations.

The CESE scheme family is summarized as,

1. the a scheme: Eqs. (3.7) and (3.8).
2. the $a-\varepsilon$ scheme or the simplified $a-\varepsilon$ scheme: Eqs.(3.7) and (3.11) or (3.17).
3. the $a-\varepsilon-\alpha-\beta$ scheme: Eqs.(3.7) and (3.13).

Among the above schemes, the last is the most complete one. Note that if setting β to zero, the $a-\varepsilon-\alpha-\beta$ s scheme is exactly the $a-\varepsilon$ scheme. As analyzed in [9], the CESE method can be used for nonlinear system as long as the stability criterion, i.e., CFL ≤ 1, while choosing ε between zero and unity.

3.2 Application of the CESE method to the MHD problem

As described in section 3.1, no eigenvector is needed for implementing the CESE method for nonlinear system compared with the other numerical methods. What needed is the eigenvalues of Jacobian matrix for monitoring the CFL number during computation. In our present computation, the CFL number based on the maximum eigenvalue is monitored to keep it below unity. As presented in section 2, the Jacobian matrix of one-spatial-dimensional MHD equations is not a homogenous one. The $a-\varepsilon-\alpha-\beta$ scheme is recommended for numerical analysis.

Since the first-order-spatial derivatives of primary parameters are taken as unknown, their initial values and boundary values should be specified for computation. Usually, they are all set to zero for initial conditions. At boundary, the derivatives are usually set according real physical nature. In our present study, the derivatives at boundaries are all set to zero unless otherwise stated. The parameters ε, α and β are set to half, unity and unity respectively.

4. Results and Discussions

4.1 Brio and Wu's Case

Proposed by Brio and Wu [1], this MHD problem has been a benchmark test for solving the one-dimensional ideal MHD equations. Similar to Sod's shock-tube problem, the initial condition is composed of two distinct states:

$$Left:\begin{cases}\rho=1.000\\ u=0.000\\ v=0.000\\ w=0.000\\ p=1.000\\ B_y=\sqrt{4\pi}\\ B_z=0.000\end{cases}\qquad Right:\begin{cases}\rho=0.125\\ u=0.000\\ v=0.000\\ w=0.000\\ p=0.100\\ B_y=-\sqrt{4\pi}\\ B_z=0.000\end{cases}$$

with $B_x=0.75\sqrt{4\pi}$, $\gamma=2$. According to [1], $\Delta x=1$ and $\Delta t=0.2$. The total time is 80. 801 grid points are used to discretize the spatial domain. Figures 2(a-e) show numerical solution of pressure, density, velocity *u*, velocity *v* and B_y.

The wave family consists of right-moving and left-moving waves. The right-moving waves include a contact discontinuity, a slow moving shock and a fast rarefaction wave. The left-moving waves include a fast rarefaction wave, and a slow compound wave, which is formed by a slow shock attached by a rarefaction wave. Our result shows sharp resolution of all shock waves. Oscillations could be seen near the trailing edges of the right-moving fast rarefaction wave and the left-moving fast rarefaction wave. The oscillations may be caused by the high-accuracy of the CESE method. Similar oscillations can also be observed at the trailing edge of the right-moving fast rarefaction wave in Jiang and Wu [5]. The structure of the slow-moving compound wave is shown in Fig. 2f. Comparisons with previously reported data at the front, the peak, and the tail of the compound wave are listed in Tables 1 to 3. The result in Xu [6] was obtained with 400 grid points. Our data at the three positions are taken from grid point No. 371, 376 and 390 respectively. The present solution compares favorably with the previous results by Brio and Wu [1].

Figure 2g shows the result of grid refinement study, in which 201, 401 and 801 grid points are used. The same CFL number is used for these three calculations. The numerical solution of using 401 grid points is nearly identical to that using 801 points. Further mesh refinement does not improve numerical accuracy. For the 201-grid-point solution, the lack of resolution is mainly in the region of slow compound wave. Present solution of this benchmark problem shows that the CESE method is capable of capturing complex MHD flow features.

4.2 Dai and Woodward's Case

Again, the initial condition of this one-dimensional problem is composed of two distinct states, listed in the following:

$$Left:\begin{cases}\rho=0.18405\\ u=3.8964\\ v=0.53610\\ w=2.4866\\ p=0.3641\\ B_y=2.394\\ B_z=1.197\end{cases}\qquad Right:\begin{cases}\rho=0.10\\ u=-5.5\\ v=0.0\\ w=0.0\\ p=0.1\\ B_y=2.0\\ B_z=1.0\end{cases}$$

with $B_x=4$ and $\gamma=5/3$. Since this case has analytical solution [3], it is often used to verify numerical schemes. In the present study, 401 grid points are used in the spatial domain according to [3]. The results shown in Figs 3(a-g) are taken at $t=0.15$. The comparison between the analytical solution and numerical result for pressure, density, velocity components (*u*, v, *w)*, and magnetic field (B_y, B_z) are presented. There are seven discontinuities in this case: moving to the left, a fast shock, a slow shock and a rotational discontinuity, moving to the right, a fast shock, a slow shock, a rotational discontinuity and a contact discontinuity.

By comparing with theoretical result in [3], again, the MHD solution with CESE method is quite good. Study on different resolution is also made. With 201 and 401 grid points, and under the same CFL condition, Figure 3h shows comparison of density profiles. The accuracy is nearly the same with different resolution.

In order to show the ability to treat the non-reflective boundary condition with the CESE method, the computation lasted to $t=1.2$. The boundary conditions at the two ends are set to the non-reflective boundary conditions. The pressure profiles at $t=0.27$, $t=0.45$, $t=0.6$ and $t=1.2$ are shown through Fig. 3i-3l respectively. All discontinuities propagate out of the computational domain.

4.3. Orszag and Tang's MHD Vortex

As our preliminary effort to apply the CESE method for multidimensional MHD problem, the Orszag and Tang's MHD vortex case is adopted here. This compressible flow proposed by Orszag and Tang contains significant features of MHD turbulence, and has taken as a standard numerical test. The flow involves complex evolution due to interactions between shock waves and the vortices. The initial condition is specified as

$$\rho(x,y,0)=\gamma^2,\ u(x,y,0)=-\sin(y),$$
$$v(x,y,0)=\sin(x),\ w(x,y,0)=0$$

$$p(x,y,0)=\gamma,\ \ B_x(x,y,0)=-\sin(y),$$

$$B_y(x,y,0)=\sin(2x),\ B_z(x,y,0)=0$$

where $\gamma = 5/3$.

The computational domain is $[0,2\pi]\times[0,2\pi]$ with periodic boundary condition in both x and y directions. We used a uniform mesh of 200×200 grid nodes. We have successfully run our calculation from $t = 0$ to $t=8$, which is the final time in most of previously published results. Note that we have run our computer program for much longer time and the calculation is stable and solution is reasonable.

For the sake of comparison, we show the density contours at $t=0.5$, $t=2$ and $t=3$ using the same contour level as that in Jiang and Wu [5]. We found that our results are almost identical to Jiang and Wu's result, obtained by using a WENO scheme. Note that Jiang and Wu adopted a correction procedure based on solving a Poisson equation to enforce the divergence-free condition of the magnetic field. This procedure maintained the integrity of the numerical solution and stabilized the calculation for long-term evolution of the MHD field. In our calculations, however, no correction step was employed and the solution quality of the magnetic field depends solely on the nature of low numerical damping of the CESE method.

Figures 4(a-c) show very complex shock structure. At $t=2$, an intermediate shock is formed at the shock front in the region of $\pi < x < 1.5\pi$ and $0 < y < 0.75\pi$. At $t=3$, the fast shock front in the region of $1.25\pi < x < 1.5\pi$ and $0.5\pi < y < 0.75\pi$, and a slow shock front in the region of $0.5\pi < x < \pi$ and $0.5\pi < y < 0.75\pi$.

5. Concluding Remarks

In this paper, we reported the extension of the CESE method to calculate the MHD equations in one and two spatial dimension. Contrast to the modern upwind schemes, the present approach has much simpler logics and operational counts. Several standard MHD problems have been solved, including Brio and Wu's one-dimensional test case, Dai and Woodward's test, and Orszag and Tang's two-dimensional test. In all cases, numerical results by the CESE method compared favorably with that obtained by using the higher order modern upwind schemes. In addition, we also demonstrated that the non-reflective boundary condition treatment of the CESE method could be straightforwardly applied to the MHD model equations.

References

1. Brio, M., and Wu, C.C., "An Upwind Difference Scheme for the Equations of Ideal Magnetohydrodynamics", *Journal of Computational Physics*, vol. 75, 1988, pp. 400-422.

2. Sabkaran, K., Martinelli, L. and Choueiri, E.Y., "A Flux-Limited Numerical Method for the MHD Equations to Simulate Propulsive Plasma Flows," AIAA paper 2000-2350, 2000.

3. Dai, W., and Woodward, P. R., "Extention of the Piecewise Parabolic Method to Multidimensional Ideal Magneto-hydro-dynamics," *Journal of Computational Physics*, vol. 115, 1994, pp. 200-212.

4. Powell, K. G., "An approximate Riemann solver for magneto-hydro-dynamics," ICASE Report 94-24, 1994.

5. Jiang, G. -S. and Wu, C. C., A High-Order WENO Finite Difference Scheme for the Equations of Ideal Magneto-hydro-dynamics, *Journal of Computational Physics*, Vol.150, 1999, pp.561-594.

6. Xu, K. "Gas Kinetic Theory Based Flux Splitting Method for Ideal Magneto-hydro-dynamics,"

Journal of Computational Physics, vol. 153, 1999, pp. 334-352.

7. Zachary, A. L., Malagoli, A. and Colella, P., A Higher-order Godunov method for multidimensional ideal *SIAM J. Sci. Comput*. Vol.15, 1994, pp.263-280.

8. Chang, S.C. and To, W.M., " A New Numerical Framework for Solving Conservation Laws – The Method of Space-Time Conservation Element and Solution Element," NASA TM 104498, 1991.

9. Chang, S.C., "The Method of Space-time Conservation Element and Solution Element – A New Approach for Solving the Navier-Stokes and the Euler Equations," *Journal of Computational Physics,* vol. 119, 1995, pp. 295-324.

10. Chang, S.C., Wang, X.Y. and To, W.M., "Application of the Space-time Conservation Element and Solution Element Method to One-Dimensional Convection-Diffusion Problems," *Journal of Computational Physics*, Vol. 165, 2000, pp.189-215.

11. Wang, X.Y. and Chang, S. C., "A 2D Non-splitting Unstructured Triangular Mesh Euler Solver Based on the Space-time Conservation Element and Solution Element Method." *Journal of Computational Fluid Dynamics*, Vol.8, 1999, pp.309-325.

12. Zhang, Z.C., Yu, S. T. and Chang, S.C., "A Space-Time Conservation Element and Solution Element Method for Solving the Two- and Three-Dimensional Unsteady Euler Equations Using Quadrilateral and Hexahedral Meshes," *Journal of Computational Physics*, Vol.175, 2002, pp.168-199.

Appendix

The Jacobian matrix is as

$$F = \frac{\partial \mathbf{f}}{\partial \mathbf{u}} =$$

$$\begin{bmatrix} 0 & 1 & 0 & 0 & 0 & 0 & 0 \\ \frac{\gamma-3}{2}u^2 + \frac{\gamma-1}{2}\left(v^2+w^2\right) & (3-\gamma)u & (1-\gamma)v & (1-\gamma)w & (1-\gamma) & \frac{2-\gamma}{4\pi}B_y & \frac{2-\gamma}{4\pi}B_z \\ -uv & v & u & 0 & 0 & -\frac{B_x}{4\pi} & 0 \\ -uw & w & 0 & u & 0 & 0 & -\frac{B_x}{4\pi} \\ A_1 & A_2 & A_3 & A_4 & A_5 & A_6 & A_7 \\ -\frac{uB_y - vB_x}{\rho} & \frac{B_y}{\rho} & -\frac{B_x}{\rho} & 0 & 0 & u & 0 \\ -\frac{uB_z - wB_x}{\rho} & \frac{B_z}{\rho} & 0 & -\frac{B_x}{\rho} & 0 & 0 & u \end{bmatrix} \tag{A1}$$

where

$$A_1 = -\gamma\frac{ue}{\rho} + (\gamma-1)u\left(u^2+v^2+w^2\right) + \frac{\gamma-2}{8\pi}\frac{u\left(B_x^2+B_y^2+B_z^2\right)}{\rho} + \frac{B_x}{4\pi}\frac{\left(uB_x+vB_y+wB_z\right)}{\rho} \tag{A2a}$$

$$A_2 = \gamma\frac{e}{\rho} - \frac{3}{2}(\gamma-1)u^2 - \frac{(\gamma-1)}{2}\left(v^2+w^2\right) - \frac{\gamma-2}{8\pi}\frac{\left(B_x^2+B_y^2+B_z^2\right)}{\rho} - \frac{B_x^2}{4\pi\rho} \tag{A2b}$$

$$A_3 = -(\gamma-1)uv - \frac{B_xB_y}{4\pi\rho} \tag{A2c}$$

$$A_4 = -(\gamma-1)uw - \frac{B_xB_z}{4\pi\rho} \tag{A2d}$$

$$A_5 = \gamma u \tag{A2e}$$

$$A_6 = -\frac{\gamma-2}{4\pi}uB_y - \frac{B_x}{4\pi}v \tag{A2f}$$

$$A_7 = -\frac{\gamma-2}{4\pi}uB_z - \frac{B_x}{4\pi}w \tag{A2g}$$

TABLE 1
Comparison of Flow Variables at the Front of Compound Wave

Method	ρ	u	v	B_y	p
Upwind [1]	0.6763	0.6366	-0.2333	0.5849	0.4574
CESE	0.6764	0.6366	-0.2334	0.5850	0.4575

TABLE 2
Comparison of Flow Variables at the Peak Point of Compound Wave

Method	ρ	u	v	B_y	p
Theory [1]	0.7935	0.4983	-1.290	-0.3073	0.6687
Kinetic [6]	0.8179	0.4679	-1.083	-0.1239	0.7300
Roe [6]	0.8257	0.4623	-0.928	0.0163	0.7300
CESE	0.8281	0.4611	-1.069	-0.1083	0.7349

TABLE 3
Comparison of Flow Variables at the Tail of Compound Wave

Method	ρ	u	v	B_y	p
Theory [1]	0.6965	0.5987	-1.583	-0.5341	0.5157
Upwind [1]	0.6963	0.5997	-1.578	-0.5341	0.5133
CESE	0.6967	0.5990	-1.584	-0.5346	0.5151

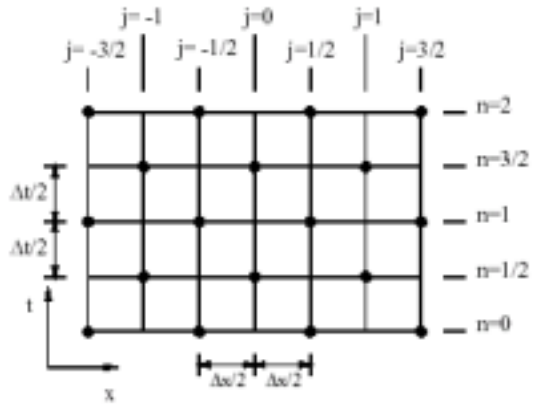

a

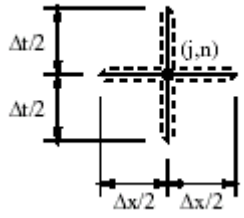

b

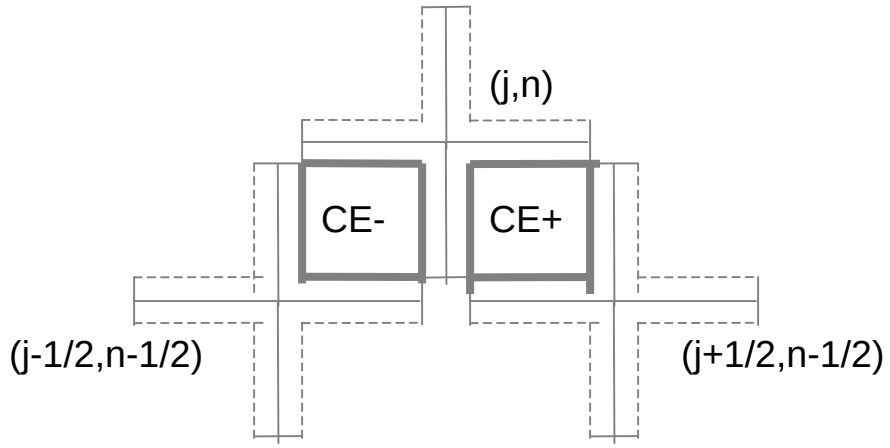

c

Fig. 1. Definition of space-time mesh, a Solution Element (SE) and Conservation Element(CE). (a). Staggered mesh arrangement in space-time coordinates. (b). Definition of SE. (c) Definition of CE.

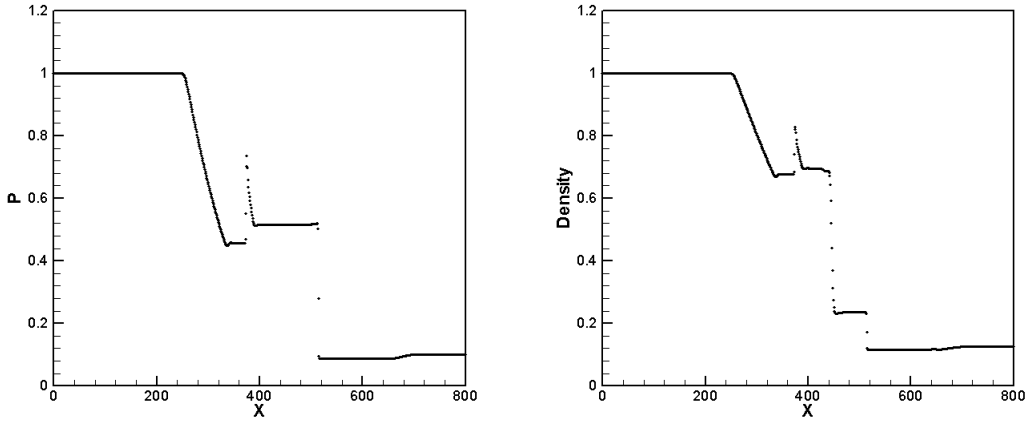

a

b

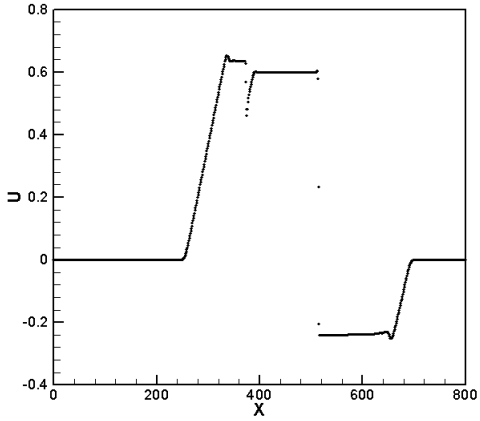

c

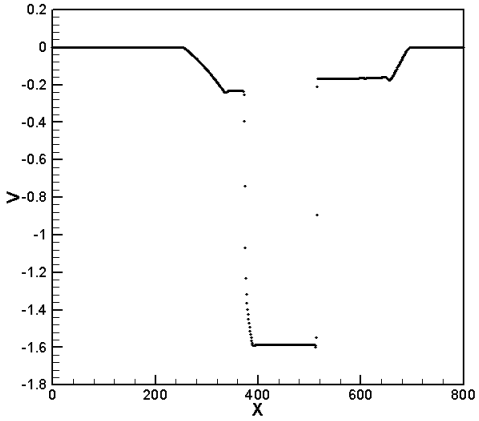

d

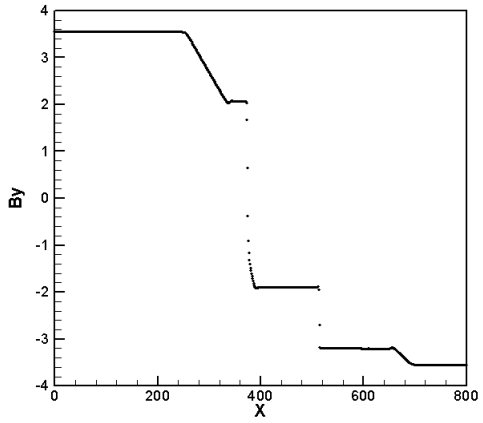

e

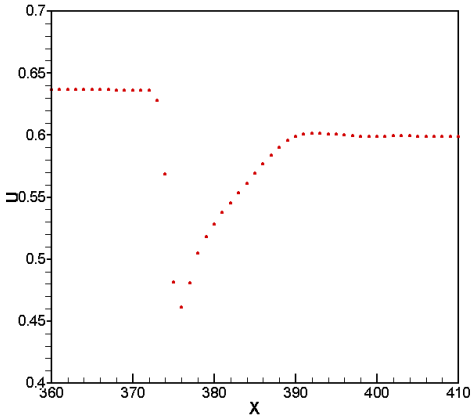

f

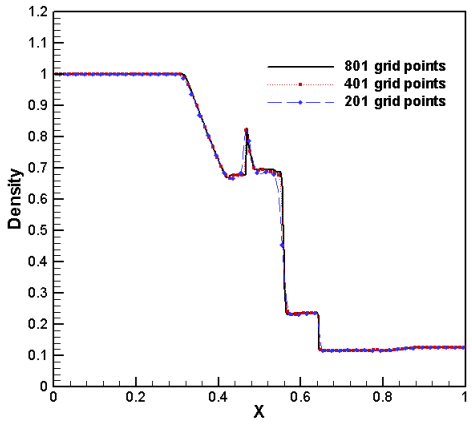

g.

Fig.2: MHD solution by the CESE method for Brio and Wu's case. (a).Pressure profile. (b). density profile (c).Velocity *u*.profile. *(*d). Velocity *v*. profile. (e).Magnetic field *By*. profile. (f). Enlarged slow compound wave. (g). Comparison between different resolution

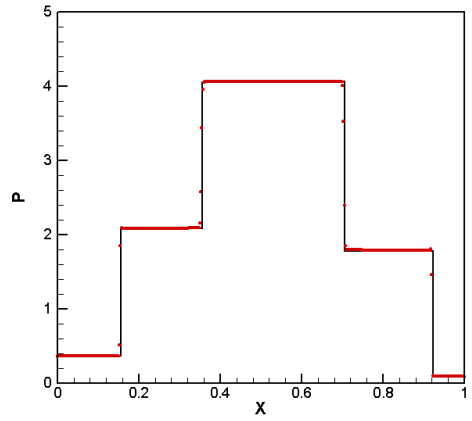

a

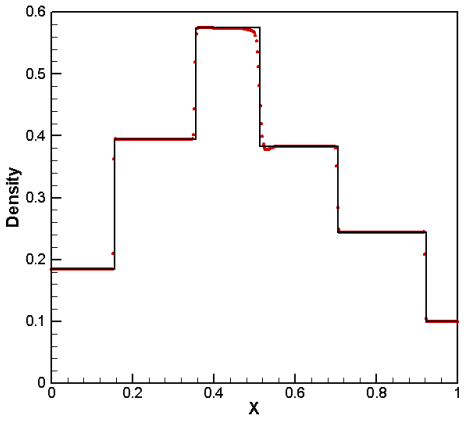

b

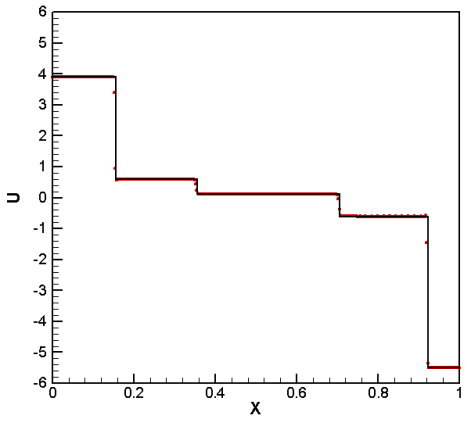

c

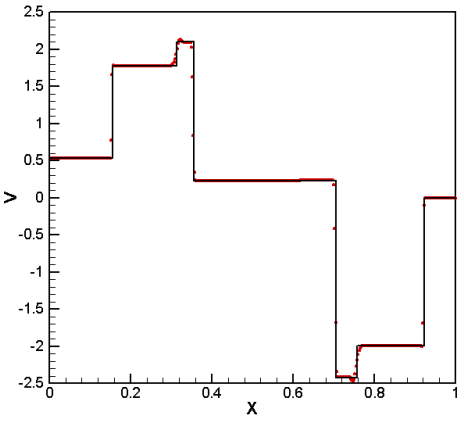

d

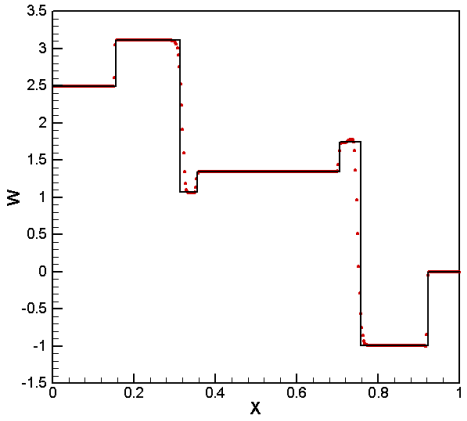

e

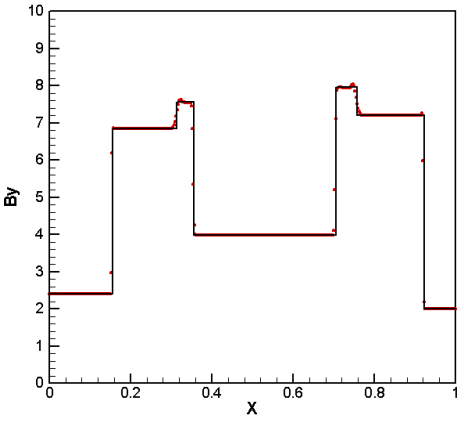

f

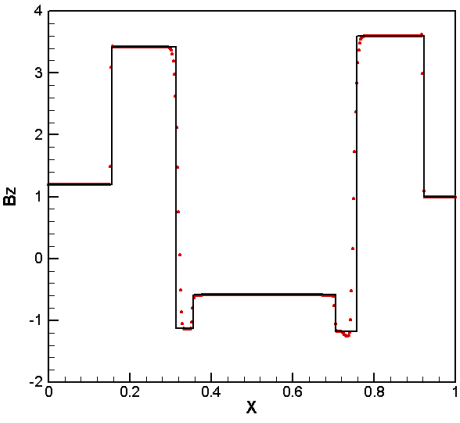

g

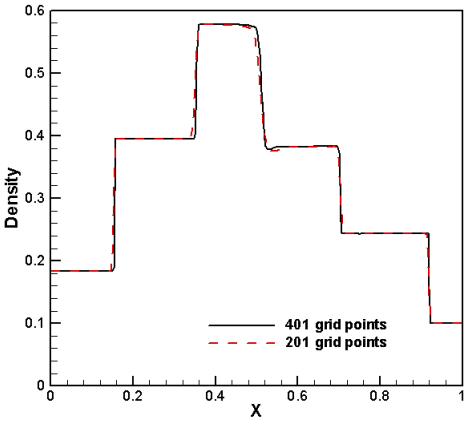

h

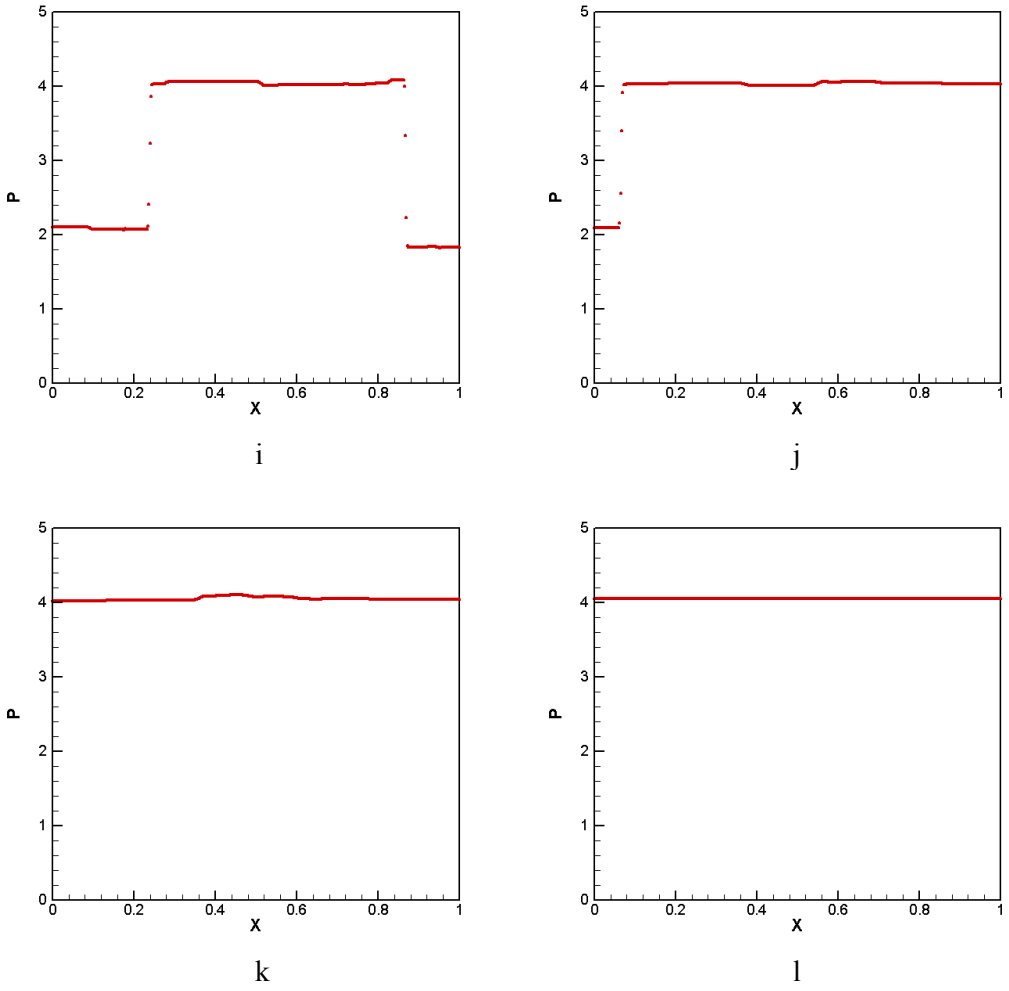

Fig.3: MHD solution by the CESE method for Dai and Woodward's case. (Solid line by the analytical solution in [3]. Dots by CESE method.)
(a). Pressure profile. (b). Density profile. (c). Velocity *u* profile. (d). Velocity *v*. profile.
(e). Velocity *w* profile. (f). Magnetic field *By*. profile. (g). Magnetic field *Bz*. profile
(h). Comparison between different resolution. (i). Pressure profile at *t=0.27*.
(j). Pressure profile at *t=0.45*. (k). Pressure profile at *t=0.60*. (l). Pressure profile at *t=1.20*.

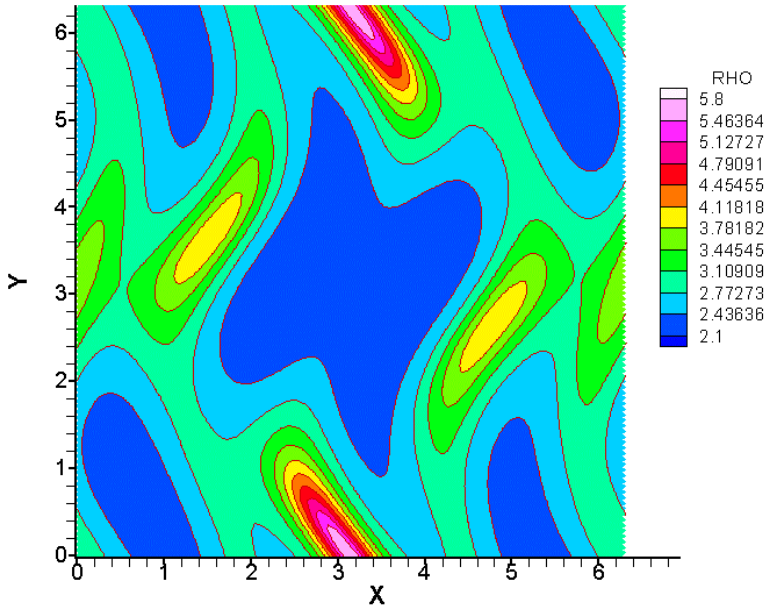
RHO
5.8
5.46364
5.12727
4.79091
4.45455
4.11818
3.78182
3.44545
3.10909
2.77273
2.43636
2.1
Y
X
0
1
2
3
4
5
6

a.

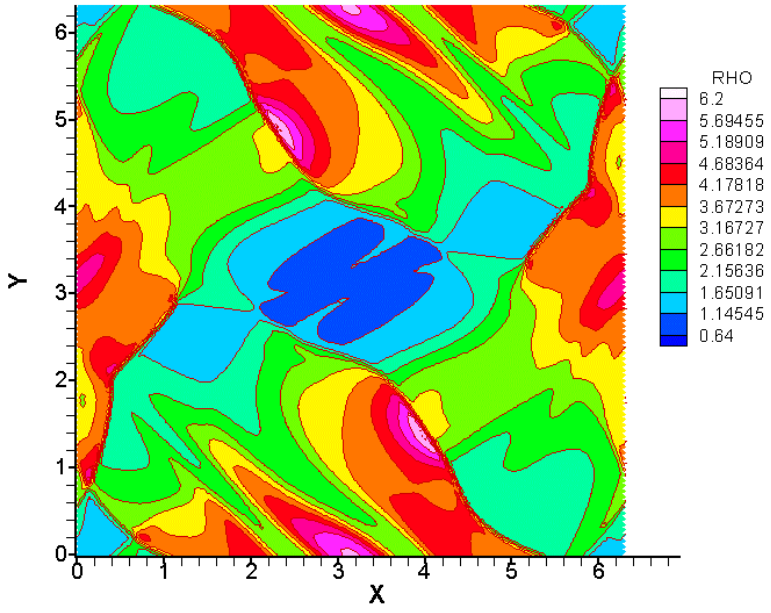
RHO
6.2
5.69455
5.18909
4.68364
4.17818
3.67273
3.16727
2.66182
2.15636
1.65091
1.14545
0.64
Y
X
0
1
2
3
4
5
6

b.

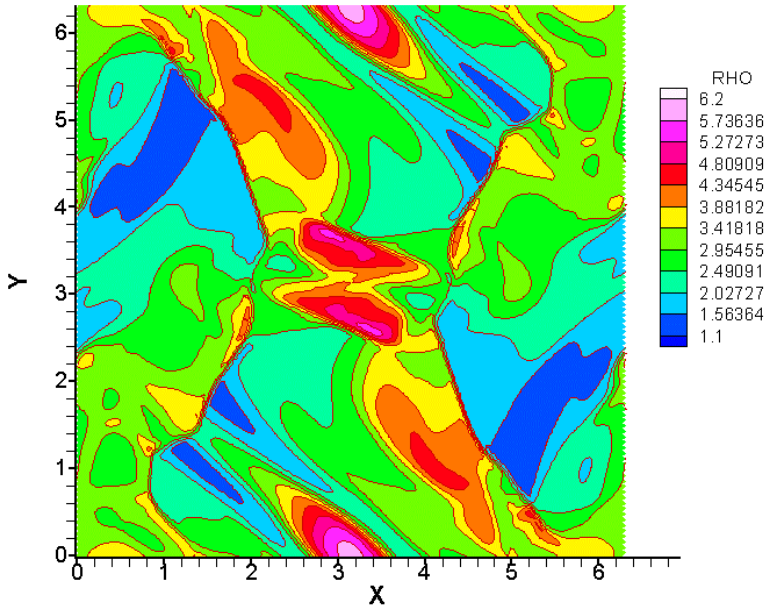

c

Fig.4: MHD Solution by the CESE method for Orzag and Tang's case.
(a). Density contours at $t = 0.5$. (b). Density contours at $t = 2$. (c). Density contours at $t = 3$.